Effect of self-modulation to optical fiber loop mirror signal on chaotic laser diode dynamics

R. ABBAS*
First Karkh Directorate of Education, Ministry of Education, Baghdad, Iraq

The laser diode (LD) signal is injected inside an optical fiber loop mirror (OFLM), which was constructed by two identical pieces of 1X2 couplers with a 10:90 coupling/splitting ratio. Two arms for the etalon are selected in such a way that the first one of them has 10% optical power and the second has 90%. Interfering two signals gives rise to signal fluctuations before emerging on two sides: backward toward the LD device and forward toward the detection then modulation. Results indicated that signal power inside OFLM is affecting the overall resulted signal in a different manner to the case of the existence of both optical feedback (OFB) and the optoelectronic feedback (OEFB). The effect of variation in optical signal strength inside OFLM and self-modulated radio frequency strength is founded on the number of output emerging signal spikes in roughly identical Poly Fit functions, which indicate the dominant type of nonlinearities. Values for these spikes fluctuated from 33 to 58 against the former effect and from 15 to 48 against the latter one. Results for chaotic dynamics associated with the LD subjected to both OFB and self-chaotic modulation, simultaneously with the application of OEFB, were found to be more sensitive in the case of pumping near the LD free-running threshold. Resulted threshold reduction values are founded changeable versus those three techniques parameters, which gives the facility to make dynamic chaotic control. The latter found application in simulating unite of optical neural network.

(Received October 19, 2024; accepted April 3, 2025)

Keywords: Optical Feedback, Optical Fiber Loop Mirror, Opto-electronic Feedback, Laser Diode, Chaotic Dynamics, Neural Network

1. Introduction

Long-distance optical fiber propagation of a chaotic light waveform is simple. It is possible for disorder to spread across hundreds of kilometers (km). Because of this property, optical chaos can be used in optical communication applications. For optical chaos communications applications, it is possible to accomplish optical amplification and dispersion compensation for chaotic optical signals [1]. Fiber optic reflectors are very desirable because of their low losses, minimal implementation complexity, and affordability. To enhance all-fiber optical system applications such fiber lasers, optical signal processing, telecoms, remote sensing, and others, all these properties are very desirable [2].

One of the most adaptable optical system topologies is the OFLM. They can be employed as mirrors or optical filters in laser and sensor applications. In mode-locked fiber lasers, the coupler's parallel or cross ports—at least one of which is made of a nonlinear medium—are connected to form two rings that serve as a mirror. We refer to these arrangements as Nonlinear Optical Loop Mirrors (NOLM). This can also be used as a mirror device with only a ring and no nonlinear media; polarization control provides the reflectivity in this case [3]. Last Ref. reported mathematical model for electric field for OFLM system clockwise (CW) and counter clockwise (CCW) two arms as the following:

$$E_{ccw} \propto E_{in}(E^{i\beta_{ccw}L_{ccw}})/\sqrt{2} \quad (1)$$

and;

$$E_{cw} \propto E_{in}(E^{i\beta_{cw}L_{cw}})/\sqrt{2} \quad (2)$$

where E_{in} is the primary electric field amplitude, β is propagation constant such that: $\beta = 2\pi n/\lambda$, n is the refractive index, λ is signal wavelength and L is the fiber arm length. Then, the intensity is given as:

$$I_{norm} \propto (E_{ccw} + E_{cw})(E_{ccw} + E_{cw})^* \quad (3)$$

The interference of these two waves results in a coherent spectrum that can be described as a cosine function. For this case, the spectral intensity is given by [4]:

$$I_{norm} \propto cos^2\left(\frac{\pi(L_{ccw}n_{ccw} - L_{cw}n_{cw})}{\lambda}\right) \quad (4)$$

Thus, signal observed from the system has an optical spectrum similar to that resulted from a traditional Fabry-Perot laser optical cavity. For FOLM the transmission and reflection intensities are measurable based on Jones matrices and reported for Sagnac FOLM interferometer in Refs. [2, 5, 6]. In case of high-Birefringence (hi-bi) optical fiber segment inserted in the FOLM, intensity pattern has a periodic dependence on wavelength given by [2]:

$$\Delta\lambda = \frac{\lambda^2}{\Delta n.L} \quad (5)$$

where Δn is the hi-bi fiber birefringence, L is the hi-bi fiber length and λ is the central wavelength. This period depends on the hi-bi fiber length and birefringence.

2. Theory

A single-mode laser model based on Maxwell-Bloch equations included three differential equations which are reported in Ref. [7]. The three relevant variables are the electric field $E(t)$, the atomic polarization $P(t)$, and the population inversion $D(t)$. They are usually decay on very different time scales, which are given by the decay rates for each last three parameters. If one of these rates is larger than the others, the corresponding variable relaxes fast and consequently adiabatically adjusts to the other variables. The number of equations describing the laser in this condition is thus reduced. This is known as adiabatic elimination of variables [7]. This phenomenon is used for the classification of lasers in terms of these decay rates to class A, B and C with one, two and three variables, respectively. A laser diode (LD) is classified as a class-B laser, for which two rate equations in solitary running are given to describe its dynamics [8]:

$$\frac{dE(t)}{dt} = \kappa\big(-1 + AD(t)\big)E(t) \quad (6)$$

$$\frac{dD(t)}{dt} = \gamma\big(1 - D(t) - E^2(t)D(t)\big) \quad (7)$$

where A is a constant; γ is decay ratio such that: $\gamma = \gamma_{\parallel}/\gamma_{\perp}$in which $\gamma_{\parallel}$ is is the decay rate of $D(t)$, and $\gamma_{\perp}$the decay rate of the atomic polarization; $\kappa = \kappa_c/\gamma_{\perp}$ is the OFB strength in which κ_c is the decay rate of the electric field in the laser cavity.

The laser intensity exhibits chaotic behavior due to nonlinear frequency mixing in the laser cavity caused by an external feedback or modulation at a frequency approaching the relaxation oscillation frequency. Thus, chaotic temporal dynamics are observable in the frequency range (few GHz) corresponding to the relaxation oscillation frequency. Laser intensity dynamics are significantly influenced by the photon-to-population inversion interaction rate. As illustrated in Fig. 1, the balance of energy provision and consumption between the population inversion (carrier density) and photons can be destroyed, especially when a portion of self-feedback light is injected into the laser cavity or when an external modulation is applied to the laser medium. In such cases, irregular intensity dynamics are expected. This is a qualitative explanation of how chaotic intensity fluctuations are generated in laser systems with extra disturbance. The external disturbance modulates the atom-photon (carrier-photon) interaction, and the laser output's chaotic intensity fluctuations are caused by nonlinear frequency mixing between the external modulation and the prolonged relaxation oscillation [8].

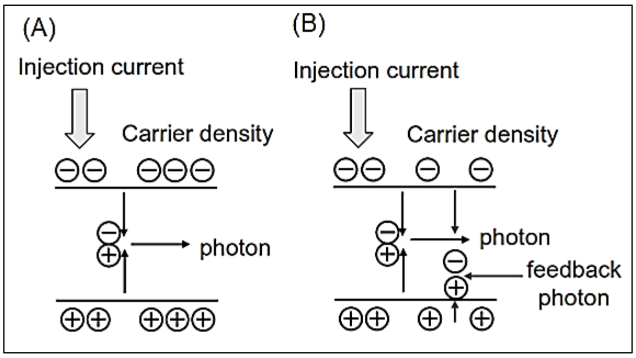

Fig. 1. Schematic of the carrier–photon interaction in a LD (A) without and (B) with OFB

The balance of the carrier–photon interaction is destroyed by the feedback photons that produce chaotic instability of laser output [8]. The frequency of relaxation oscillation (f_r) is proportional to the square root of the normalized pump power divided by both lifetimes of carrier and photon [8];

$$f_r = \frac{1}{2\pi}\sqrt{\frac{p-1}{\tau_p\tau_s}} \quad (8)$$

where p is the pumping power normalized by the lasing threshold value, τ_s is the population inversion lifetime, and τ_p is the photon lifetime in the laser cavity.

Therefore, it depends on the semiconductor medium's properties. As mentioned above, LDs typically have f_r values of a few GHz. Conversely, the external cavity length—in this case, the loop mirror length—determines the external cavity frequency (f_{ext}), which is dependent on the distance between the laser cavity's facet and the external mirror:

$$f_{ext} = \frac{C}{2nL_{ext}} \quad (9)$$

where L_{ext} is the external cavity length (one-way), n is the refractive index in the external cavity, and C is the speed of light.

The external cavity frequency corresponds to the inverse of the round-trip time of light propagation in the external cavity. Note that it is useful to memorize that the light takes 1 ns to propagate the distance of 0.3 m in vacuum. The nonlinear interaction between f_r and f_{ext} results in the quasiperiodic route to chaos as the feedback strength increases.

In addition, the delay time (τ) of the OFB signal enhances the complexity and chaos of the laser dynamics. This is due to the time-delayed feedback system being considered a high-dimensional dynamical system. Related with frequency modulation contribution in output emission, an optical chirp is defined as a sudden change of the center wavelength of a laser, caused by laser instability. When an optical transmitter is intensity modulated, the corresponding frequency modulation is called frequency chirp. When an optical signal travels through a dispersive medium, frequency chirp typically causes further performance loss and widens the modulated optical signal's spectral broadness. Suppose that an optical field that has both intensity and phase fluctuations [9]:

$$E(t) = \sqrt{P(t)}e^{j\varphi t} = j\varphi t + 0.5lnP(t) \qquad (10)$$

where $P(t) = |E(t)|^2$ is the optical power.

In equation (10), the real part inside the exponent is 0.5 $ln\ P(t)$ and the imaginary part is $\phi(t)$. The following ratio is equivalent to the ratio between the phase modulation and the intensity modulation, which is defined as the chirp parameter:

$$\alpha_{1W} = 2\frac{d\varphi(t)/dt}{dlnP(t)/dt} = 2P\frac{d\varphi(t)/dt}{dP(t)/dt} \qquad (11)$$

Ref. [10] reported analytical results for the Lang-Kobayashi system both Kolmogorov–Sinai (KS) entropy and Kaplan–Yorke (KY) dimension as a function of κ or L_{ext}. For k both the KS entropy and KY dimension increase monotonically in the chaotic region as κ is increased. This result implies that both complexity and dimensionality of the chaotic attractor increase monotonically with increase of the feedback strength κ. While for L_{ext} the KY dimension increases almost linearly as the L_{ext} is increased, whereas the KS entropy maintains a constant value of the chaotic region. This result indicates that the complexity is almost the same, while the dimensionality is linearly increased with the increase of delay time. The KS entropy and KY dimension are good indicators to quantify the complexity and dimensionality of nonlinear dynamical laser systems [11, 12, 13].

Various OFB signal types can be employed to create deterministic disorder. An OFB with polarization rotation can be helpful in creating chaos. The two orthogonal polarization modes of the electric fields interact nonlinearly in this method, where the polarization of the laser output is rotated at a 90-degree angle. Chaos can also be generated in LDs using an OEFB signal. A photodetector detects the laser output and transforms it into an electrical signal. The injection noise receives feedback of the electronic signal.

The nonlinear behavior in an OFLM, or figure-eight OFLM, created by joining the output components of an interferometer coupler serves as the foundation for all-optical switching geometry devices. Because the phase velocity is intensity dependent, the propagation of light will no longer be the same for the two paths if the power coupling ratio is not equal to 1/2 [14]. The high-intensity components of a pulse are transmitted when it propagates via the nonlinear loop mirror, while the low-intensity portions are reflected and rejected by the optical isolator. The pulse changes shape and sharpens after a few round trips. An additional application for the nonlinear loop mirror with OFB is as an all-optical recirculating fiber-loop memory [15, 16]. A synchronized probing pulse at a different wavelength can be used to selectively and nondestructively read out the content of the fiber-loop memory.

When operating for continuous wave radiation, the device differs significantly from its pulse operation because nonlinear interference between the input and feedback powers needs to be taken into account.

Recently, chaotic dynamics in LDs based on filtered optical feedback is experimented for artificial networks by Refs. [17, 18, 19, 20, 21] and extended to include laser network synchronization [22, 23]. In order to increase chaoticity, the Lyapunov exponent must increase to guarantee hyper chaos. This is done by following mixed and hybrid feedback and injection techniques [24].

The complex systems seen in nature are full of fascination. However, it can be very difficult to identify signs of determinism in their high-dimensional dynamics due to both noise and system information gaps. Merely one or a small number of pertinent variables can be measured with a restricted temporal and/or geographical resolution. An effective method for researching these kinds of systems is to concentrate on describing their dynamics at the event level, taking intervals between occurrences, for example. Neural inter-spike intervals, heartbeat-to-heartbeat intervals, waiting durations for earthquakes, intervals between peaks in social network communication, etc. are a few examples of this methodology. Ordinal analysis is a symbolic method used to analyze these occurrences that takes into account the relative order in which they occur. Current study focuses on spectrum analysis, including time series inter-spike intervals for several measurements. This method is based on calculations for spectrum-specific characteristics, such as statistics for the time series number of spikes (peaks). Compare these statistics with analysis methods published in the literature, such as Refs. [25] and [26], which proposed a computing method for the probabilities of symbolic patterns. The stochastic optical system in such operation is subjected to OFB from the OFLM and also an OEFB represented by the self-modulation.

The investigated configuration set-up employed an optical fiber coupler interferometry; its type is classified as a Sagnac interferometer, shown in Fig. 2 [2], with a 1×2 optical fiber coupler instead of the 2×2. This is to receive a reflected field from LD output and transmit the output field toward a photodetector before re-injecting it again from its bias. Noting that the hi-bi optical fiber is replaced with optical attenuator.

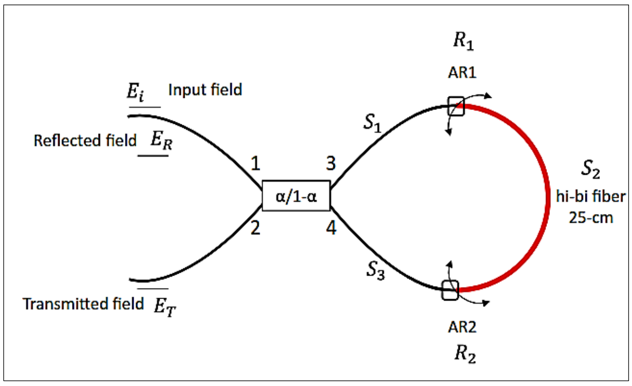

Fig. 2. Sagnac optical fiber interferometer

3. Experimental set-up

In this experimental study, as shown in the following Fig. 3 (A), an LD source with a center wavelength of 1310 nm and commercial code (BT-1VF-R) is installed. The LD output is directed to a 10:90 optical fiber directional coupler (OFDC1). For last component, the 90% ratio port is connected with an optical fiber attenuator (OA) which transmit optical signal to port with 90% from a second 10:90 optical fiber directional coupler (OFDC2). It is also connecting the remaining 10% of the two ports together to complete the OFLM. Output for the OFLM is directed toward a photodetector (PD) followed by a power divider. The first of the two resulted ports for the power divider are going to a mixed signal oscilloscope (MSO), while the second is connected with a radio frequency attenuator (RFA); its function is to control the opto-electronic feedback (OEFB) that is uploaded to the LD supplied electric power. In this situation, the LD receives instability from its front by the OFLM, i.e., backward optical power, and from behind as an RF signal. Real configuration set-up is shown in the same figure (B).

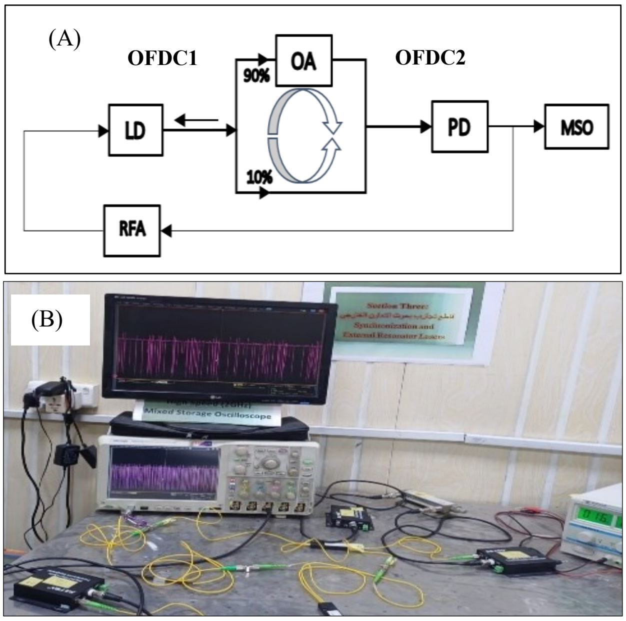

Fig. 3. Configuration set-up (A) and its photo-plate during experiment run (B). LD is the laser diode device, PD is a photodetector, RFA is the radio frequency Attenuator, and MSO is the mixed signal oscilloscope, OA is an optical attenuator (colour online)

Selection for such a setup is to modify an optoelectronic circuit mixing dynamics released from an optical fiber loop mirror and self-modulation or optoelectronic feedback. This included using simple components and optics.

4. Results and discussions

A. Effect of optical signal strength inside the FOLM

The circulated signal inside the FOLM, given in Fig. 2, is constructed by connecting the two directional couplers of optical fiber, as mentioned in the experimental set-up section, which already has two parts: clockwise CW rotated and counter clockwise CCW rotating parts. To observe the effect of signal optical contribution on output dynamics, measurements were carried out on the output of OA after recording the creative observe signal from the MSO, i.e, signal identical to chaotic behavior. Results for those creatively observed signals are shown in Fig. 4 in its time series form for ten values. Analysis for these results is carried out to screen their Fourier spaces (Fast Fourier transformations (FFT)) and phase spaces. The two later analyses give the confirmation for how dynamics take effects and growth after interacting with the self-LD cavity. Two constructed field equations are reported in both equation (1) for the CCW part and equation (2) for the CW part, respectively. Subsequently, the resulted intensity is governed by equation (3), in which there exists a large difference in optical power, i.e., the two fields also have a large difference in their values. This difference will affect the expected interference pattern that was constructed from the standing wave pattern. Then each variation in optical strength for the signal with 90% contribution will give rise to that pattern. In this situation, the output spectrum can have different characteristics with each recorded observation. Experimentally, it is confirmed based on this theory that there exists a new spectrum with each new optical strength for the operating limit enclosed between -37.03 and -18.86 dBm. The time series for all entirely mentioned values inside subfigures represents fluctuated amplitudes signals under the effect of interference between the CW and CCW signals parts inside the FOLM.

The resulting spectral resolution for the longitudinal mode spacing, as given in Ref. [27], can be calculated by using two equations, $C/2\Delta L_{ext}$ and $\Delta\upsilon = C/2nL_c$ for the external and entire laser, two cavities. In which C is speed of light in vacuum is $3 \times 10^8 m/S$ while inside optical fiber medium it equals C/n, ΔL_{ext} is the external cavity length, FOLM, variation, n is the LD active region effective refractive index, and L_c is the LD interior cavity length. Accordingly, for the current system, the standard quantum well Fabry-Perot LD cavity length value is 300 um, the refractive index value for a fiber core is around 1.5. Calculations for the last two parameters give: 3.460 GHz for frequency separation (free spectral range) inside the LD and 13.15 MHz for the external one. Then it is needed to observe the MSO time series dynamics range for the first cavity is 0.288 nS and 0.076 nS for the interior and external cavities, respectively.

The time duration for the recorded signals is selected to be located in a microsecond (uS) range, which is equivalent to a frequency range of megahertz (MHz). Based on this frequency duration, the resulted dominant frequencies are those for the external cavity, FOLM, modes. As it is shown in Fig. 4, observed spikes (peaks) in the time series are very close to each other's in the lowest measured optical powers inside the FOLM, then tend to be gradually divergent between each other with increased measured optical power from -33.89 dBm to -25.21 dBm. After the last value, the time series returns to be included closer spikes until the highest measured optical power value: -18.68 dBm. In case of Low Frequency Fluctuations (LFF) in LD with OFB operating regime, the intensity pattern displays abrupt spikes: the intensity suddenly drops to minimum and then slowly recovers. Analysis for number of spikes against OFLM measured power is given in Fig. 5, in which, the polynomial function is satisfied for recorded results. The last is considered a power function that is characterized by having a single term from the product of a real number, coefficient, and variable raised to a fixed real number power. With such a power function the LD dynamics approved entering chaoticity emission state or instability regime. Such a regime affected by optical power of OFLM in polynomial manner.

Solitary LD dynamical rate equations ((1) and (2)) could not describe the optical system any more. Alternative is to temporarily consider the Lang and Kobayashi model [22], the most popular model included in theory, which is associated with low and moderate feedback strengths. But LD in them is subjected to only OFB. The slowly varying complex electric field and the carrier density are affected by several enterer and external parameters. One of the external parameters is feedback coupling coefficient and feedback delay time that are both controllable in the current experiment via OFLM interferometer that is linked by equations (1) to (4) in the theory section. In order to complete the physical scenario, equations for chaotic modulation, such as theory reported by Refs. [28, 29]) should be introduced to discussions. The modulation in this set-up represents a signal that came from LD itself but passed through the OFLM and suffered from attenuation before doing the interference. Accordingly, the uploaded signal is different than the originally generated signal from the LD device.

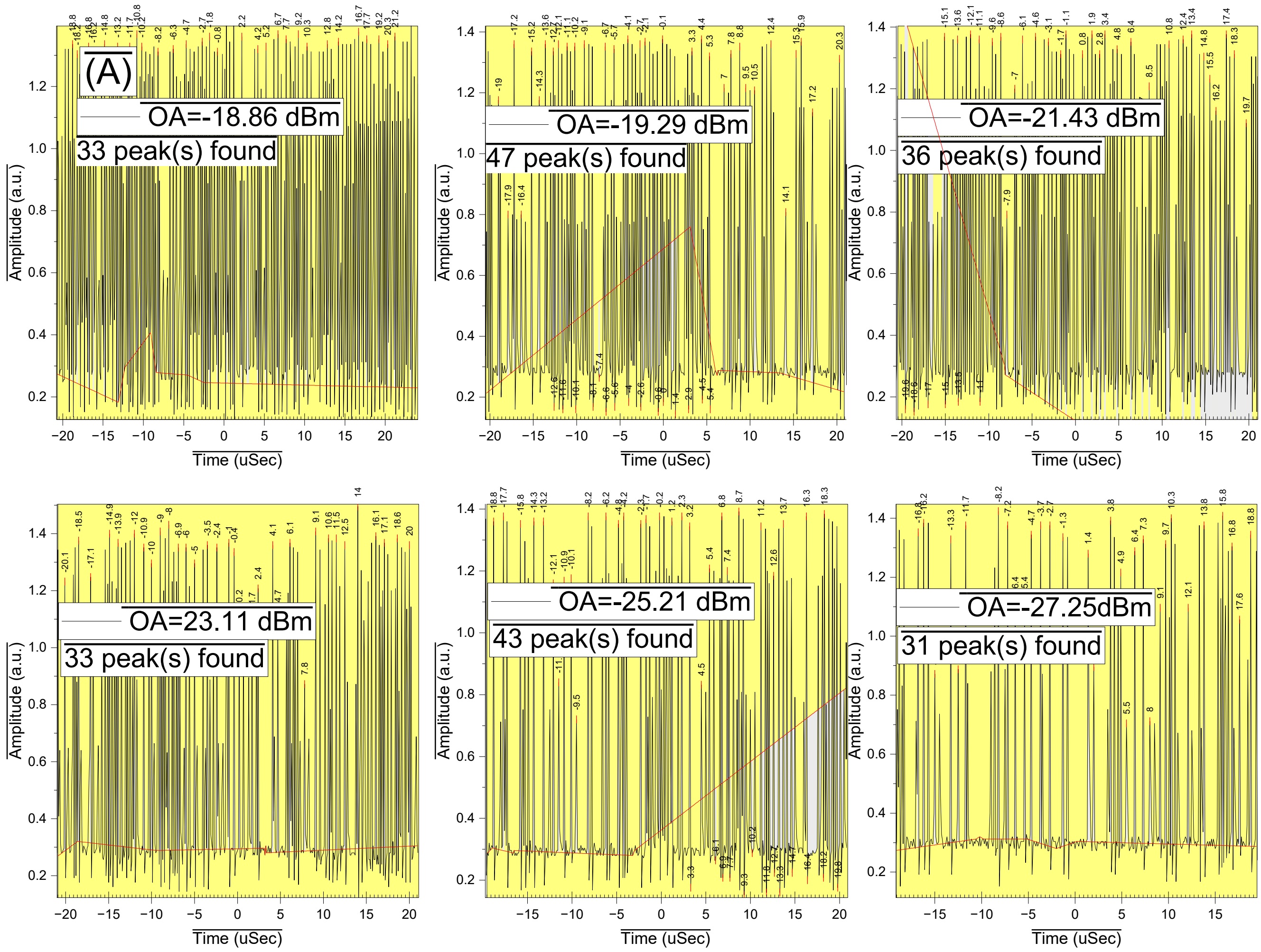

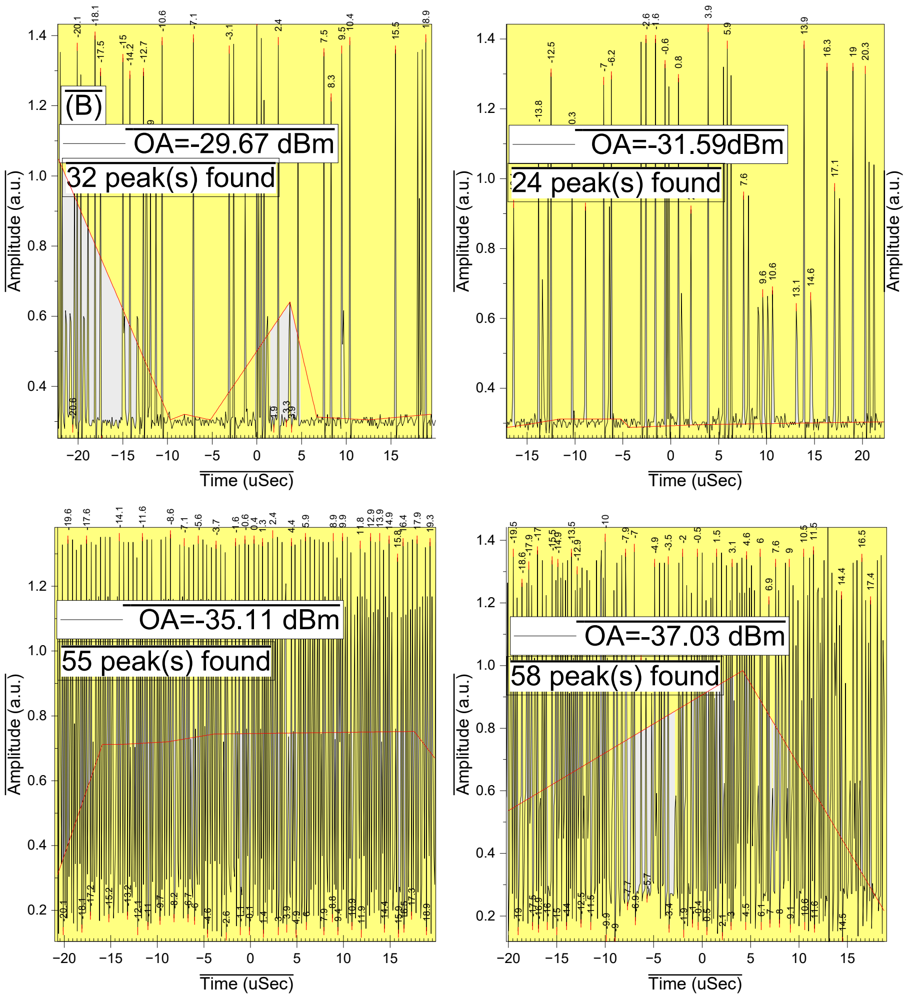

Fig. 4. Time series for observed signals with measured OA values inside OFLM from (reported in its legends): (A) -18.86 to -27.25 dBm, and (B) -29.67 to -37.03dBm, when self-modulated is applied to LD (colour online)

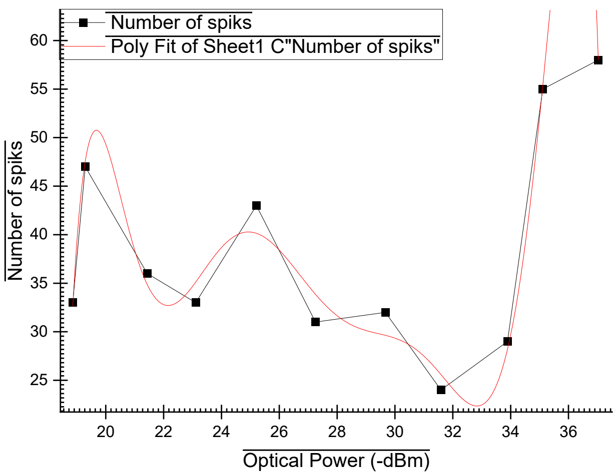

Fig. 5. Statistics for time series number of peaks (spikes) behavior against measured optical power from inside OFLM (colour online)

For the same observed time series that had been shown in Fig. 4, the calibrated attractors are composed by plotting the time series amplitude against the calculated derivative for the same time series, as given in Fig. 6. Attractor or phase space gives indication on how dynamical system will behave in the future, i.e., gives approval that chaoticity permanently exists in it. From Fig. 6, one finds that attractors associated with measured optical power values ranging from -18.86 to -23.11 dBm are filled attractors. Filling the attractor means that it includes an infinite number of loops. Each loop in this calibration represents lasing mode, then the LD system after subjecting to this OFLM and modulation being fully chaotic with last power values. Remaining recorded attractors tend to be half-filled in their center area of the shapes. Thus, they emit with two and several multiplications of routs to chaos nonlinearity. In such operation, the LD system and its active medium have several instabilities instead of its solitary single instability.

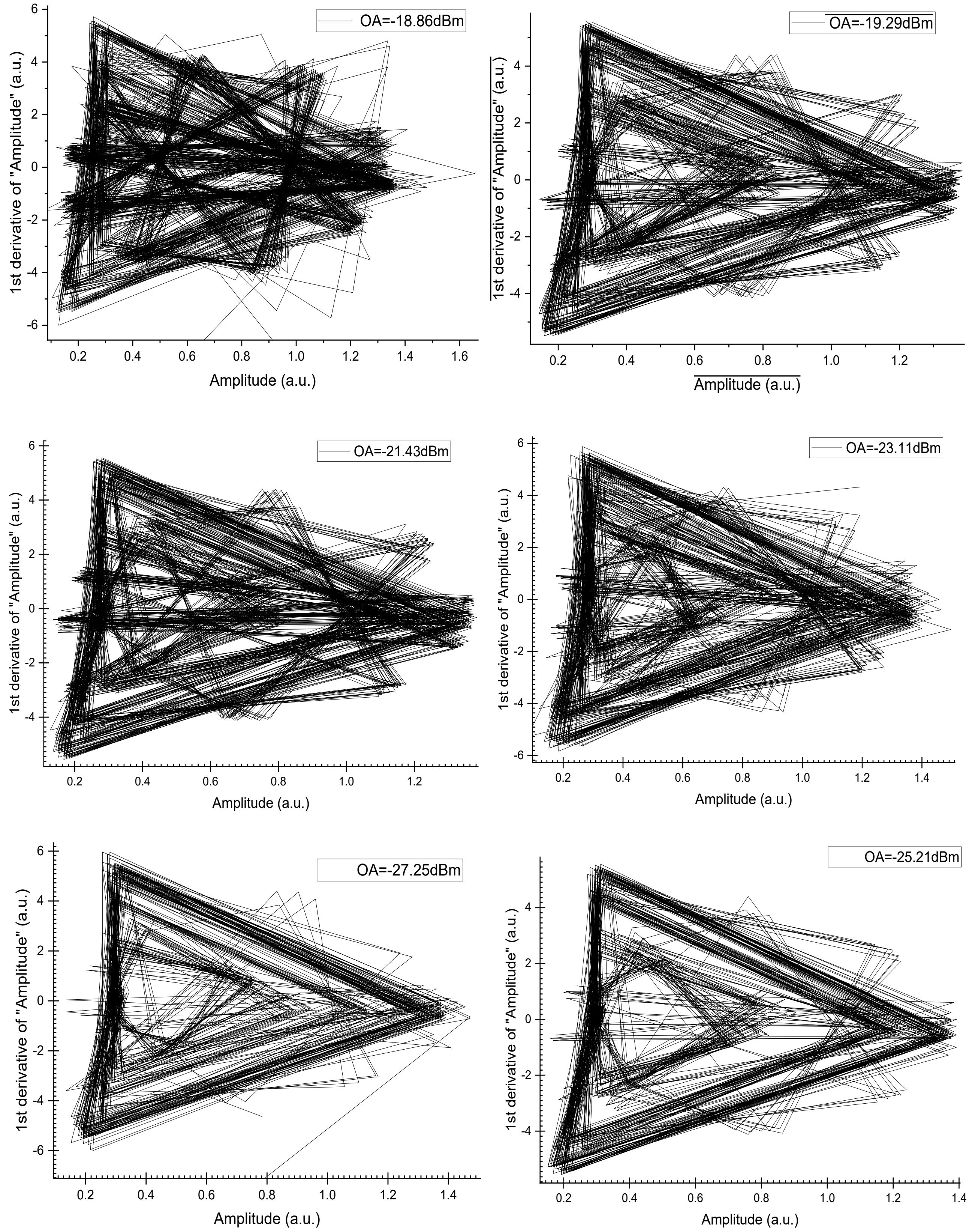
OA=-18.86dBm
OA=-19.29dBm
OA=-21.43dBm
OA=-23.11dBm
OA=-27.25dBm
OA=-25.21dBm
1st derivative of "Amplitude" (a.u.)
Amplitude (a.u.)

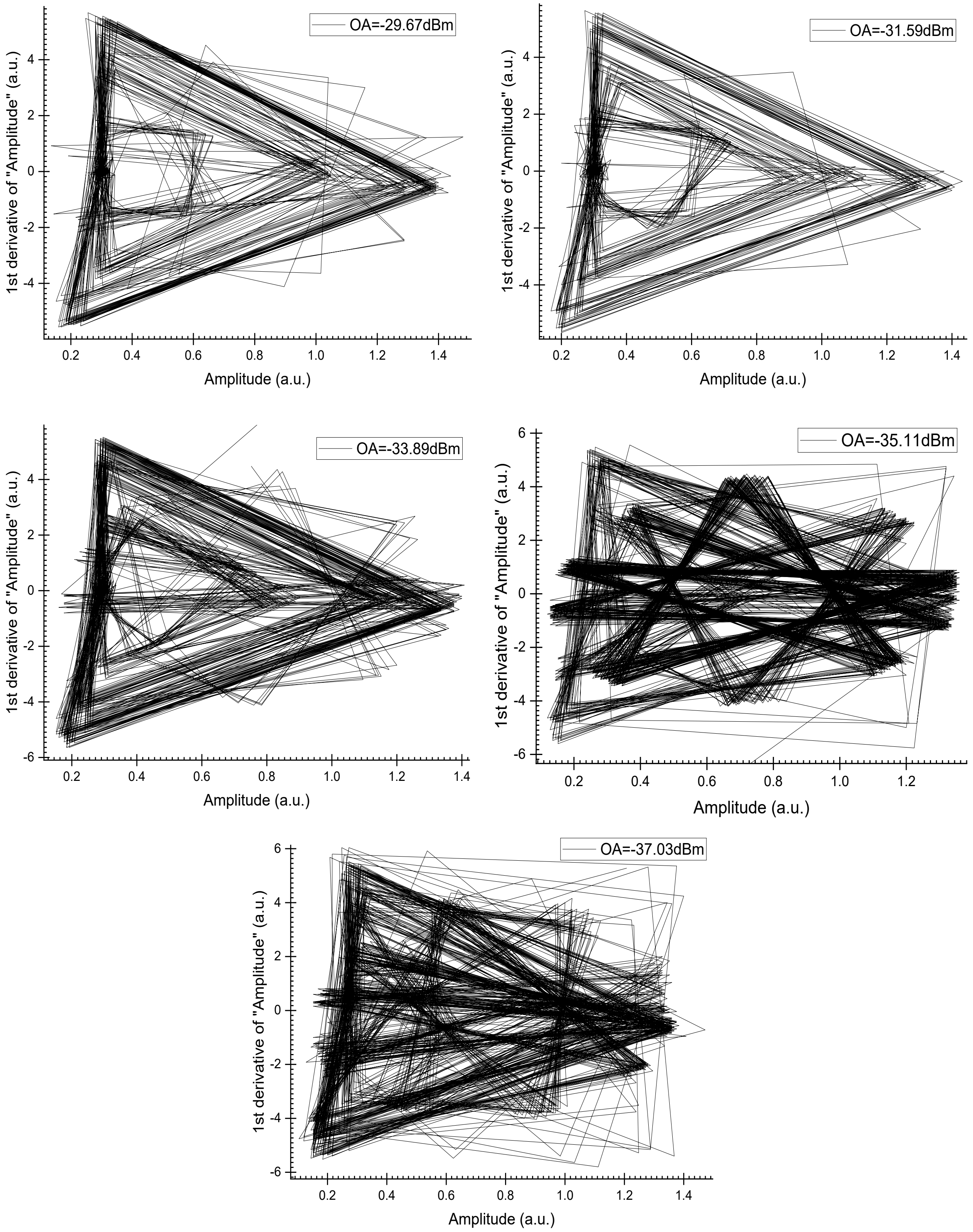

Fig. 6. Attractors for observed signals with measured OA values inside OFLM from -18.86 to 30.03 dBm, consecutively reported in legends, when self-modulated to LD

To observe LD lasing frequencies, calculations for fast Fourier transformation are required for the same time series that are given in Fig. 4. Majority of the resulting spectra, Fig. 7, show route to chaos and subjected to coherence collapse such that extended frequency spectrum is observed in the range of MHz, which, as reported earlier, matches the theoretical (Ref. [31]) expected frequency range for the external cavity (OFLM). Center frequency (F_o) is observable in the case of maximum applied OA (OA = -18.86 dBm) given in the last-mentioned figure. Whilst, no distinguished peak is found in any applied OA value. These power spectra confirm this observation. This indicated that "range of dynamics" is located at all in MHz order. This indicate that "range of dynamics" is located at all in MHz order, and confirms the impact of such an interferometer on resulting dynamics.

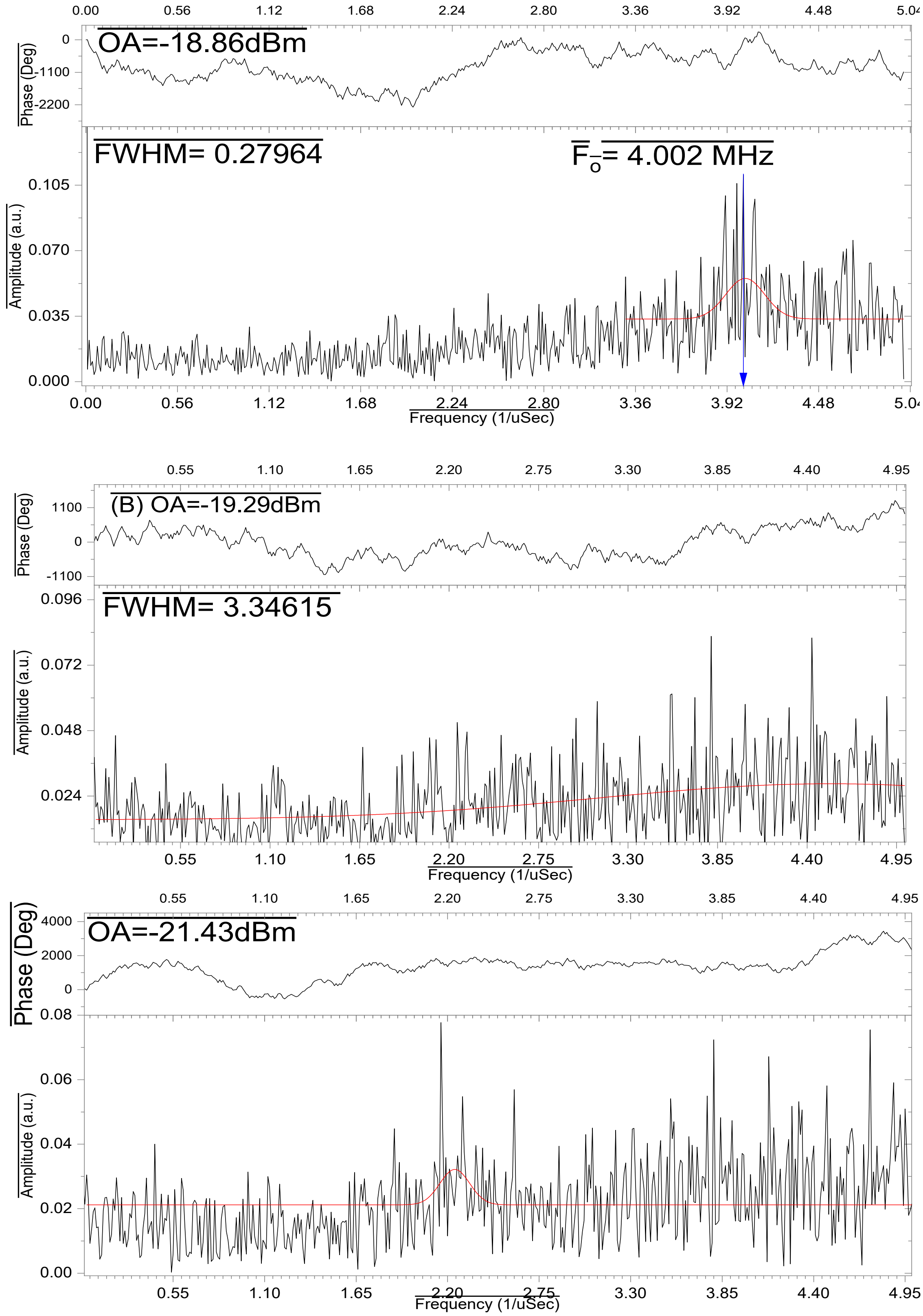

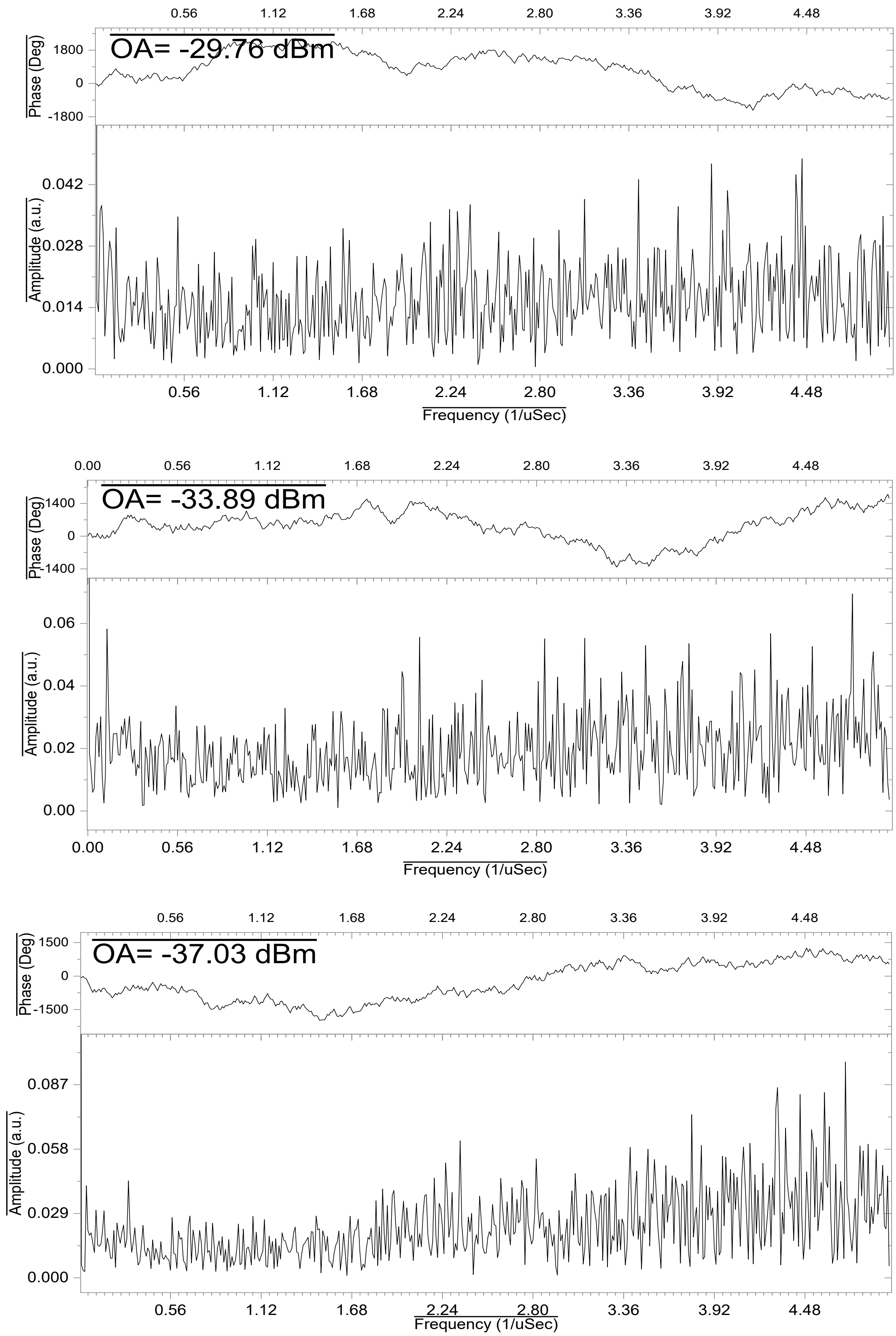

Fig. 7. Fourier spaces for observed signals with measured OA values inside OFLM from -18.86 to -37.03 dBm, consecutively reported in legends, when self-modulated to LD

B. Variation of RF signal strength after the OFLM

After two signal parts doing circulation inside the OFLM, which gives the output signal, the new constructed signal is detected and controlled by an RF attenuator. Attenuator gives the facility of tuning modulation strength before upload to the LD device. Signal RF power control affects modulation current I(t) directly during the sinusoidal amplitude, included in the second term for the following relation [28]: $I(t) = I_b + I_m\Psi_m(t)$. In the last equation, I_b and I_m are bias and modulation currents for the LD device.

It is observed from the time series in Fig. 8 that the signals are wider than those observed in part (A) of this section. The difference comes from the variation of signal RF strength, not the optical signal inside the OFLM. This means that the contribution of optical strength inside the OFLM gives rise to chaoticity for the resulted signal. This is even though the system transformed from continuous wave emission to pulsation in the last regime. In this figure, dynamics are transported from time scale to neighbored within the MSO range, i.e., variation in applied frequency modulation shifted the LD dynamics with variation in overall signal shape according to emitted frequency (stretched and compressed signal). Another variation is that related to the number of peaks, while amplitudes are conserved in the same range for all resulting signals.

The relationship between RF power and the calculated number of peaks (spikes) is shown in Fig. 9. In which the relation fitted polynomial function, i.e., starts with periodic increase with strong RF modulation then jump to polynomial higher increase with lower RF modulation strength representing pulsation. The LD system feeds itself from the OFLM in a constant manner, while the variation is located in the RF part from the modulated signal. This implies that a step decrease in modulated signal strength gives rise to periodic variation in the number of peaks.

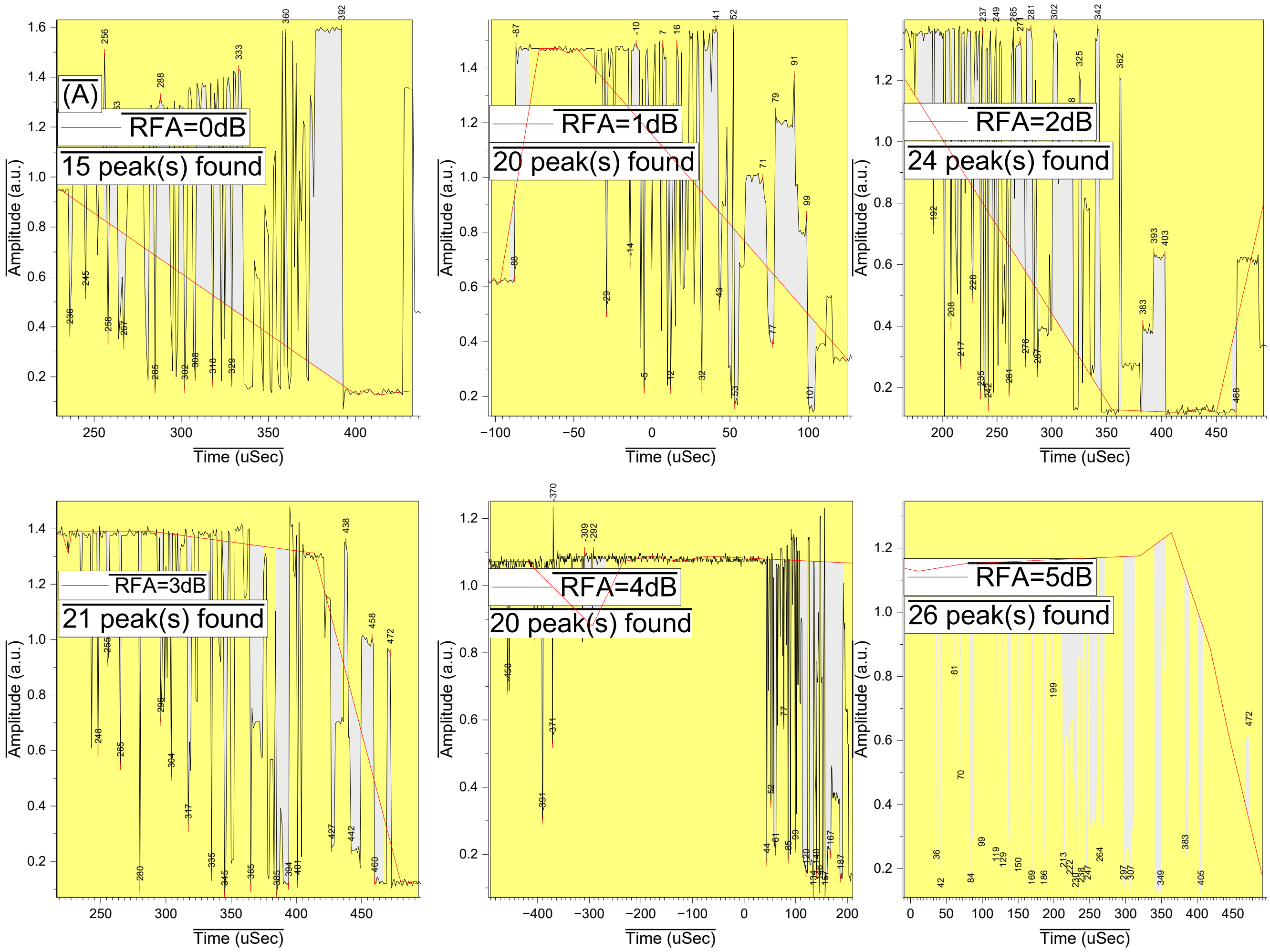

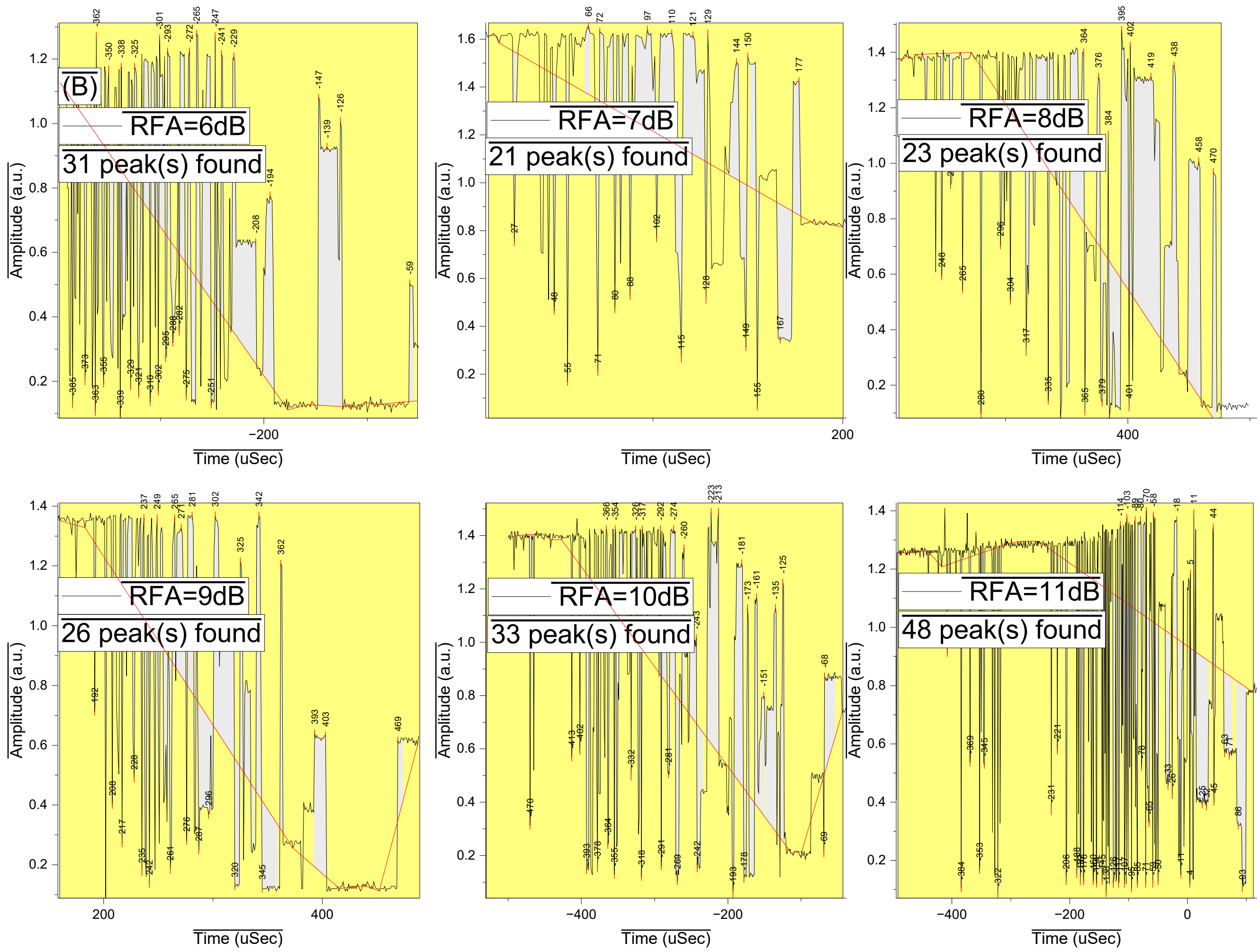

Fig. 8. Time series for observed signals with applied RFA values (after emerging from OFLM) RFA values from 0 to 5 dB (A) and 6 to 11 dB (B), when self-modulated is applied to LD (colour online)

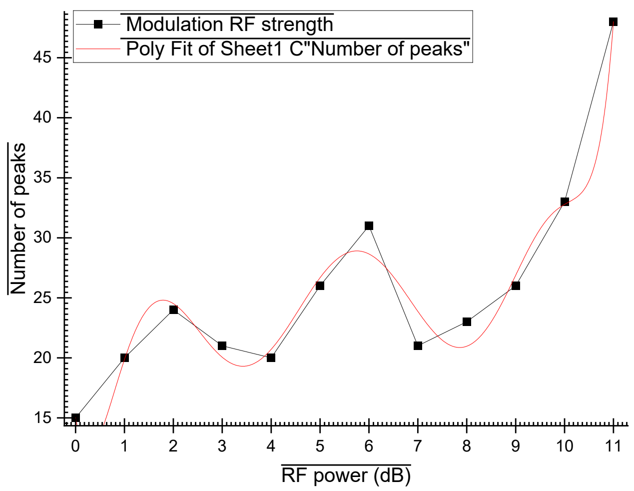

Fig. 9. Overall relation (statistics) for number of peaks (spikes) against RF attenuation for self-modulated LD. Eleven runs are carried out during the experiment (colour online)

Attractors for all-time series are also constructed and given in Fig. 10, in which all phase space areas have less filled with loops than those associated with Fig. 6. This gives indication that the contribution of optical power value for OFLM is more effective than modulation RF power level. This means that the expected number of modes or frequencies in the LD system in the future will less fluctuate within a dynamics bandwidth. The modulation current in LD is represented in first term that located in the electron time rate for the set of LD rate equations given in Ref. [30]. In which the electron density linearly proportional with injection current, when gain and electron life time and remains parameters are considered constants. Whilst expected future behavior for the system gives inverse indication to this prediction, as shown in Fig. 10 with less RFA (0 dB) and large RFA (11 dB). The LD system experimental attractors disagreed in two extremes, minima and maxima, for RF attenuation. While agreed in moderate attenuation values. This can be interpreted via self-modulation to the LD device, which is affected by OFB in addition to modulation, which gives a new degree of freedom. Injection and feedback are predicted as an effective tool in giving such freedom in LDs as it is convenient in literature such as Ref. [29]. Making comparison with photon density in this active medium system based on photon density time rate of change in earlier reference, its variation is linearly proportional to the gain. The gain in this set-up is increased via OFB, which is constant in this results part. Enthought, it applied additional gain ratio to the device via this freedom degree. As a result, a combination between two parameters (chaotic modulation and OFLM back-direction flow) resulted in such a dynamic.

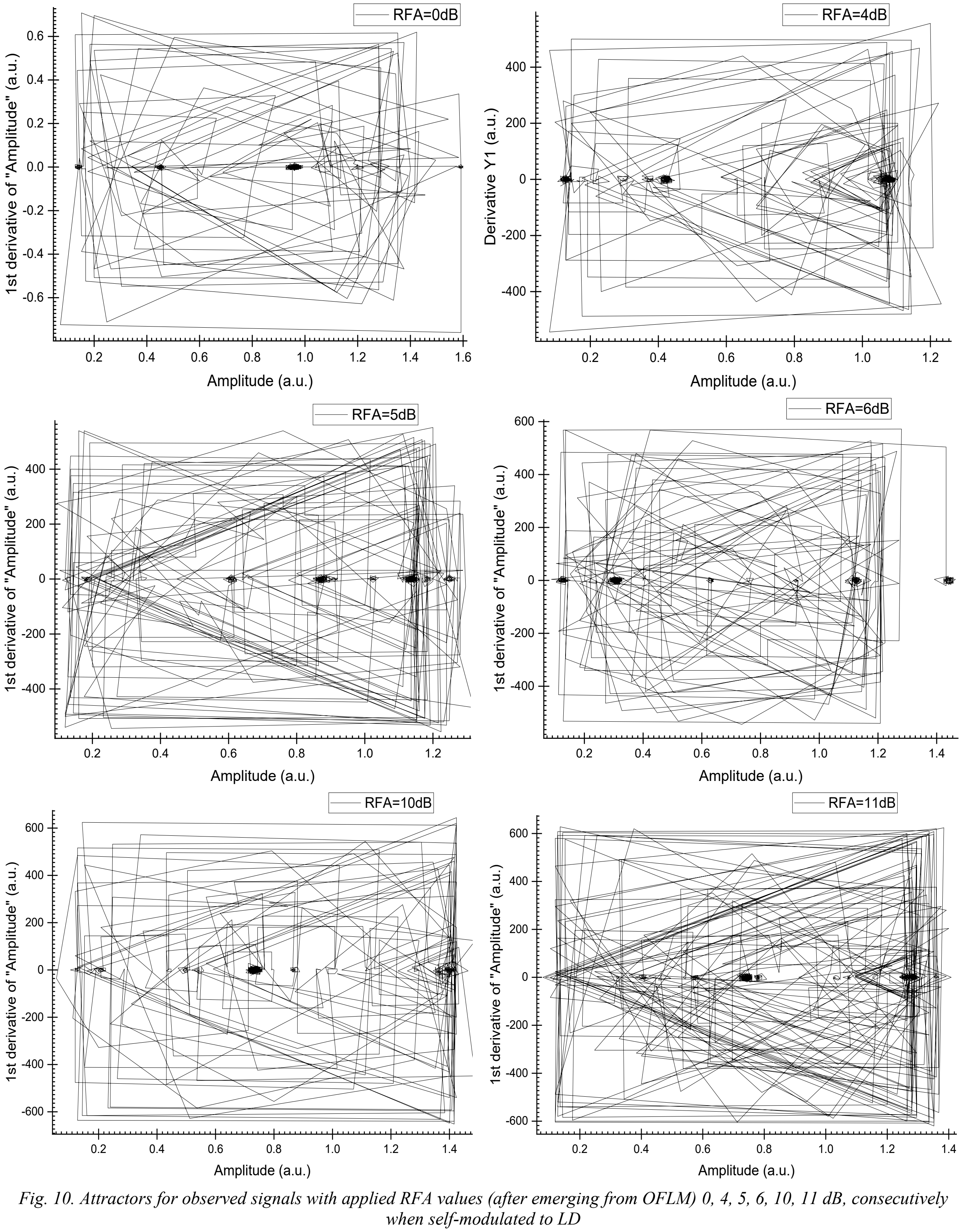

Fig. 10. Attractors for observed signals with applied RFA values (after emerging from OFLM) 0, 4, 5, 6, 10, 11 dB, consecutively when self-modulated to LD

Observations for Fourier space spectra shown in Fig. 11 confirm less perturbation affecting the system and also less noise level in these spectra. Thus, application of modulation gives rise to stable pulsation for the LD. This is clearer with the spectrum given in the same figure in RFA equaling 5 dB. In such a spectrum, the laser is an absolutely sharp frequency spectrum, i.e., the laser system is locked to only one lasing mode. Comparisons between all three tools of observations, time series (Fig. 8), attractors (Fig. 10), and FFTs (Fig. 11), respectively, give even the slight system variation in dynamics. The last mentioned RFA-applied value has a coherent time series; its attractor is triangular-shaped, contrary to all remaining attractors. This agrees with its measured FFT, which has only a sharp unique frequency.

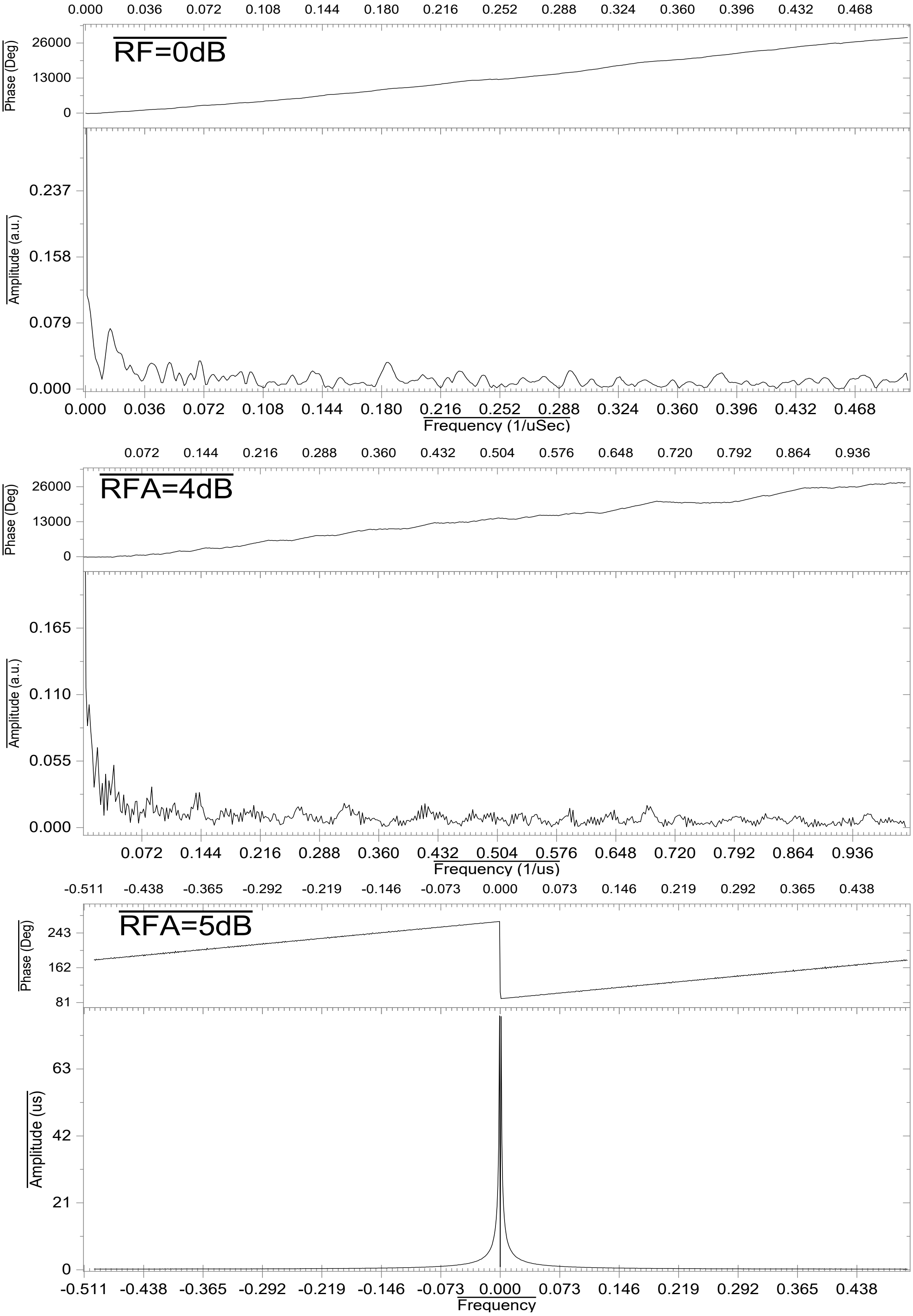

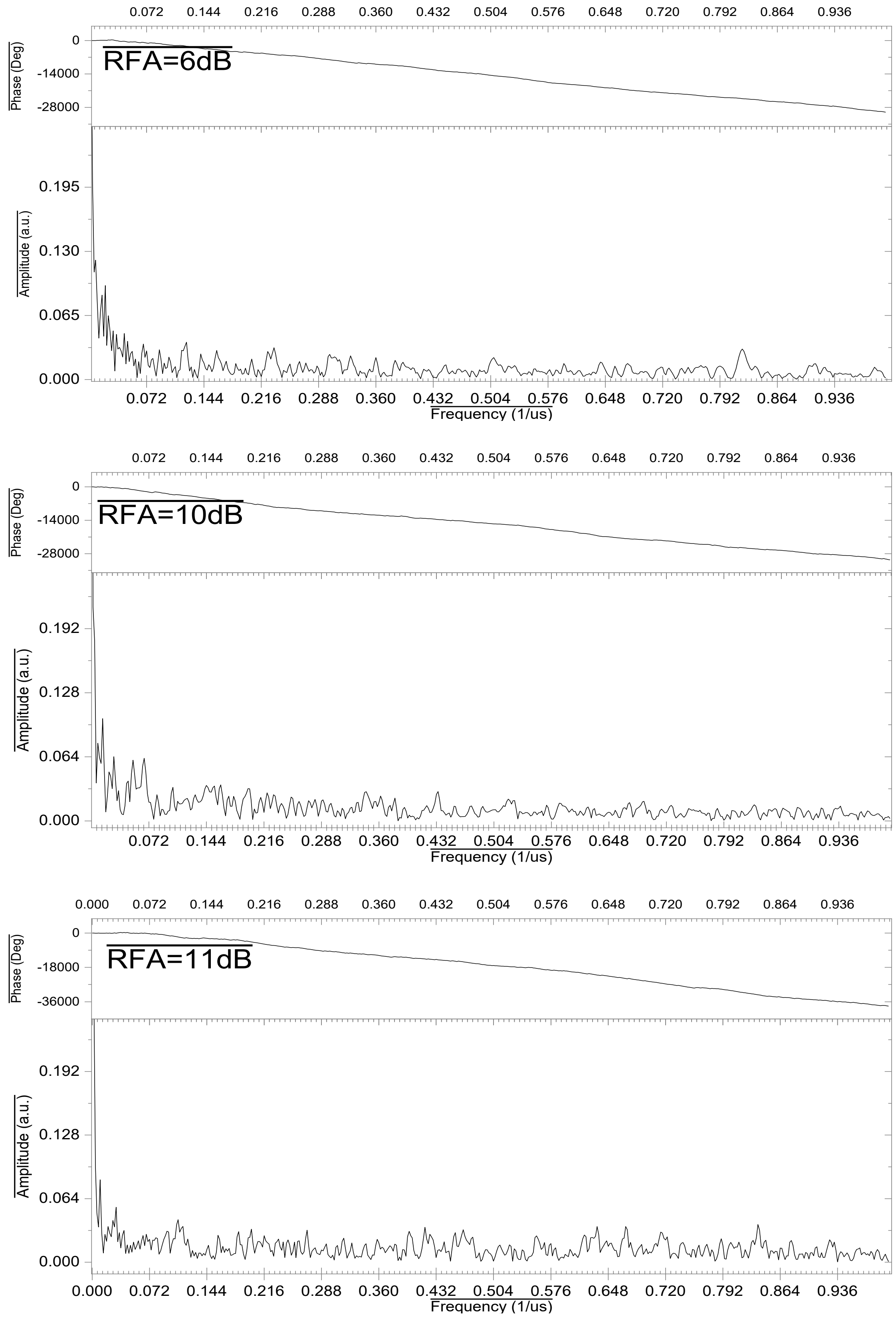

Fig. 11. Fourier spaces for observed signals with applied RFA values (after emerging from OFLM) 0, 4, 5, 6, 10, 11 dB, consecutively when self-modulated to LD

Based on observed spectra for the LD under effects including both RFA (detected signal uploaded to LD bias) and OA, the LD response showed sensible modifications in emitted spectra. The feedback mechanism can be calibrated as a data learning term in the machine learning process. In the case of feedforward, the concept is included in the same setup; configuration can be optimized to calibrate a primary network unit-based control system. This is to approve the relation between the amplitude and phase in the LD device spectra. Analysis of the input laser signal and output can give evidence for applied parameters weight in such a layer.

A neural network is a well-known structure made up of several layers of nodes, each of which conducts an affine translation of the output of the layer before it is activated by a nonlinear function, usually a rectified linear unit or a sigmoid to execute machine learning tasks.

The nonlinear activation in the current setup is simulated as a laser active medium subjected to new degree of freedom by the application of OA and RFA.

5. Conclusions

Variation in optical power circulated within the OFLM, permitting part of the output signal to be directed toward the LD device, making the device very sensitive to signal optical power. Under this parameter, a frequency chirp is observed for the laser system signal. Chirping is changed for a frequency duration period located in the MHz range. This observation confirmed that OFLM modes were more predominant than those generated from the entire LD cavity. From the other hand, variation of RF attenuation for the output signal from that interferometer with the existence of constant OFB applied to the LD translated the device to operate in fewer frequencies to a unique lasing frequency. Predictions for the future state of this system are calibrated and indicated as large perturbed compared with less perturbed in both OFB alone and OEFB with a constant OFB.

Acknowledgments

Author would like to thanks First Karkh Directorate of Education, Ministry of Education-Iraq for support and Mustansiriyah University for cooperation.

References

[1] A. Argyris, D. Syvridis, L. Larger, V. Annovazzi-Lodi, P. Colet, I. Fischer, J. García-Ojalvo, C. R. Mirasso, L. Pesquera, K. A. Shore, Nature. **438**(17), 343 (2005).
[2] I. Armas-Rivera, L. A. Rodriguez-Morales, G. Beltrán-Pérez, M. Durán-Sánchez, M. V. Andrés, B. Ibarra-Escamilla, Opt. Laser Tech. **140**, 107070 (2021).
[3] P. Robalinho, B. Soares, A. L. Ribeiro, S. Silva, O. Frazão, Sensors **23**(2), 618 (2023).
[4] P. Robalinho, O. Frazão, Photonics **8**(1), 23 (2021).
[5] P. M. R. Robalinho, B. S. Carneiro, A. L. Ribeiro, S. D. Silva, O. J. Frazao, Sensors **23**(2), 618 (2023).
[6] K. S. Lim, C. H. Pua, N. A. Awang, S. W. Harun, H. Ahmad, Progress In Electromagnetics Research C **9**, 101 (2009).
[7] P. Mandel, Theoretical Problems in Cavity Nonlinear Optics, Cambridge: Cambridge University Press, (1997).
[8] A. Uchida, Optical Communication with Chaotic Lasers Applications of Nonlinear Dynamics and Synchronization, Weinheim - Germany: Wiley-VCH Verlag & Co. KGaA, Boschstr, 2012.
[9] R. Hui, M. O'sullivan, Characterization of optical devices, in Fiber-Optic Measurement Techniques (Second Edition), Academic Press, pp. 297-446, 2023.
[10] E. Ott, Chaos in Dynamical Systems 2nd edition, Cambridge: Cambridge University Press, 2002.
[11] A. Namajūnas, K. Pyragas, A. Tamaševičius, Physics Letters A **201**(1), 42 (1995).
[12] A. Namajūnas, K. Pyragas, A. Tamaševičius, Physics Letters A **204**(3-4), 255 (1995).
[13] R. Vicente, J. Dauden, P. Colet, R. Toral, IEEE Journal of Quantum Electronics **41**(4), 541 (2005).
[14] C.-X. Shi, Optics Communications **107**(3-4), 276 (1994).
[15] H. Avramopoulos, N. A. Whitaker, Optics Letters **18**(10), 22 (1993).
[16] N. A. Whitaker, M. C. Gabriel, H. Avramopoulos, A. Huang, Optics Letters **16**(24), 1999 (1991).
[17] M. M. Jaber, A. A. Hemed, Fiber and Integrated Optics **43**(6), 235 (2024).
[18] M. Dhyaa, A. Hemed, H. Rasheed, AIP Conf. Proc. **3036**, 050020 (2024).
[19] D. R. Madhloom, A. A. Hemed, S. M. Khorsheed, East European Journal of Physics **2**, 267 (2023).
[20] Z. R. Ghayib, A. A. Hemed, Optoelectron. Adv. Mat. **16**(7-8), 307 (2022).
[21] D. R. Madhloom, A. A. Hemed, S. M. Khorshed, Iraqi Journal of Science **66**(1(SI),) 469 (2025).
[22] R. S. Abbas, Z. R. Ghayib, W. A. Jabbar, A. A. Hemed, Journal of Optics (2024). https://doi.org/10.1007/s12596-024-01858-2.
[23] A. Hemed, R. Abbas, M. Fdhala, Optoelectron. Adv. Mat. **18**(3-4), 120 (2024).
[24] R. Abbas, A. Hemed, AIP Conf. Proc. **2593**, 020004 (2023).
[25] C. Quintero-Quiroz, T. Sorrentino, M. C. Torrent, C. Masoller, SPIE photonics Europe - Proceedings Volume **9892**, Semiconductor Lasers and Laser Dynamics VII; 98921T, Brussels, Belgium, 2016.
[26] A. Aragoneses, S. Perrone, T. Sorrentino, M. C. Torrent, C. Masoller, Scientific Reports **4**, 4696 (2014).
[27] J. Keeley, J. Freeman, K. Bertling, Y. L. Lim, R. A. Mohandas, T. Taimre, L. H. Li, D. Indjin, A. D. Rakić, E. H. Linfield, A. G. Davies, P. Dean, Scientific Reports **7**, Article number: 7236 (2017).
[28] M. F. Ahmed, A. H. Bakry, F. T. Albelady, Int. J. New. Hor. Phys. **1**(1), 1 (2014).
[29] A. A. Hemed, T. Ackemann, H. J. Kbashi, B. T. Chead, J. Phys.: Conf. Ser. **1818**, 012027 (2021).
[30] J. C. Cartledge, G. S. Burley, Journal of Lightwave Technology **7**(3), 568 (1989).
[31] G. V. Tartwijk, D. Lenstra, Quantum and Semiclassical Optics: Journal of the European Optical Society Part B **7**(2), 87 (1995).

*Corresponding author: rashaasalah83@gmail.com